arXiv:cond-mat/0009288 v2 13 Feb 2001

Ab initio study of $BaTiO_3$ and $PbTiO_3$ surfaces in external electric fields

B. Meyer and David Vanderbilt
Department of Physics and Astronomy,
Rutgers University, Piscataway, New Jersey 08854-8019, USA
(February 13, 2001)

For the ferroelectric perovskite compounds $BaTiO_3$ and $PbTiO_3$, we have studied the effects of external electric fields on the structural properties of the (001) surfaces. The field-induced changes in the surface interlayer spacings and bucklings have been calculated using a first-principles ultrasoft-pseudopotential approach, and the change of the polarization and the ferroelectric distortions in the surface layers have been obtained. The surfaces are represented by periodically repeated slabs, and an external dipole layer is included in the vacuum region of the supercells to control the electric field normal to the surfaces. The influence of the electrical boundary conditions on the ferroelectric properties of the slabs is discussed. In the case of a vanishing internal electric field, our study indicates that even very thin slabs can show a ferroelectric instability.

PACS numbers: 77.55.+f, 68.35.Bs, 77.22.Ej, 77.84.Dy

I. INTRODUCTION

In recent years, ferroelectric (FE) compounds based on the cubic perovskite structure ABO_3 have attracted much interest because of their promising potential for a series of technological applications. Just to mention two examples from semiconductor industry, their ferroelectric properties can be used to build non-volatile random access memories, and their high permittivity makes them good candidates to replace SiO_2 in large-scale integrated circuits. Because of the ongoing miniaturization in semiconductor devices, this may be soon required in order to be able to construct capacitors with sufficient capacity (for example in DRAM cells) and to maintain gate oxide layers in MOSFETs which are thick enough to prevent tunneling of electrons between the gate electrode and the channel.

In these applications it is the aim to apply the FE materials in very thin film geometries where the ferroelectric and dielectric properties will be strongly influenced by surface effects. For the understanding of the behavior of FE thin films it is therefore important to explore how the FE order parameter couples to the surface. In many experimental investigations of thin films, a degradation of the FE properties has been observed. It has been believed that decreasing the thickness of thin films suppresses ferroelectricity and eliminates it altogether at a nonzero critical thickness which has been estimated to be approximately 10 nm for $PbTiO_3$.[1] However, in recent experiments, Tybell and coworkers have shown that for high-quality films of $Pb(Zr_xTi_{1-x})O_3$, a stable polarization perpendicular to the surface persists down to film thicknesses of 40 Å or less.[2] This suggests that the previously observed suppression of ferroelectricity in thin films is not a purely intrinsic effect caused solely by the presence of the surface, but is related to extrinsic factors like perturbations of the chemical composition of the surface (impurities, oxygen vacancies or other defects), surface induced strains, or variations in electrical and mechanical boundary conditions.

To investigate this further, we have studied slabs of isolated, ideal (i.e., clean and defect-free) thin films of $BaTiO_3$ and $PbTiO_3$ in (001) orientation. Both possible surface terminations (on BaO/PbO or TiO_2 layers) have been considered. It is the aim of this study to determine whether thin films of this kind still show a ferroelectric instability, and how the ferroelectric distortions and the spontaneous polarization change at the surface.

A few theoretical investigations in this direction have already appeared. In Refs. 3 and 4 we have studied the (001) surfaces of $BaTiO_3$ and $PbTiO_3$ for the case of the tetragonal axis (i.e., the direction of the spontaneous polarization) lying *parallel* to the surface. Although the surface relaxation energies are found to be substantial (i.e., many times larger than the bulk ferroelectric well depth), it turned out that the influence of the surface upon the FE order parameter is only modest. For the TiO_2–terminated surface of $BaTiO_3$ and the PbO–terminated surface of $PbTiO_3$, a modest enhancement of the FE order was found at the surface; for the other two surfaces, a small reduction in the FE distortions was observed. However, in all cases the ground state was ferroelectric, and deviations of the FE distortions from the bulk value were confined to the first few atomic surface layers.

On the other hand, for thin PZT films the experimental investigations of Tybell have shown a polarization *perpendicular* to the surface. In this case, theoretical calculations have to deal with the additional problem of the correct electrical boundary conditions far from the surfaces. In two previous studies on $BaTiO_3$,[5,6] slabs of truncated bulk material with a net polarization perpendicular to the surface have been used. The slabs were either repeated periodically, assuming periodic boundary

conditions for the electrostatic potential, or were treated as isolated slabs with a vanishing *external* electric field, and in neither case were the atoms allowed to relax fully from their ideal bulk positions.

We point out in this paper that these situations are rather artificial and do not provide useful information about the FE properties of the slabs. Instead, we will show that the appropriate electrical boundary condition is a vanishing electric field *inside* the slab. This implies that if the slab shows a spontaneous polarization, an external electric field has to be applied to compensate the depolarization field caused by surface charges. A vanishing internal electric field is equivalent to the so-called *short-circuit* boundary conditions, where the thin film is sandwiched between grounded plates of a capacitor.

Short-circuit boundary conditions have been used by Ghosez and Rabe[7] in a microscopic effective-Hamiltonian study of $PbTiO_3$ thin films. They found that (001)-oriented films with thicknesses as low as three lattice constants have a perpendicularly polarized ferroelectric ground state with a significant enhancement of the polarization at the surface. However, in the effective Hamiltonian, no information about the structural relaxation of the surface layers was included. With the present *ab initio* calculations, we confirm the finding of Ghosez and Rabe about the ferroelectric ground state, but we also show that the atomic relaxations at the surface significantly modify the effective-Hamiltonian picture of the polarization in the surface layers.

The paper is organized as follows. In Section II we describe the technical details of our computational method and the geometry of the slabs. We also discuss how to deduce the correct electrical boundary conditions and how to apply these in the supercell calculations. In Section III we present the results of our calculations on various slabs exposed to external electric fields. Finally, the paper ends with a summary in Section IV.

II. THEORETICAL DETAILS

A. Method of calculation

As in our previous studies on perovskite surfaces,[3,4,8] we have carried out self-consistent total-energy calculations within the framework of density-functional theory[9] using the Vanderbilt ultrasoft-pseudopotential scheme.[10] In the pseudopotential generation the semicore Ba $5s$ and $5p$, Pb $5d$, and Ti $3s$ and $3p$ orbitals have been included as valence states (for more details on the pseudopotentials see Ref. 11). The electron wave functions were expanded in a plane-wave basis set including plane waves up to a cutoff energy of 25 Ry. As has been shown in previous studies, this cutoff energy is sufficient to obtain well converged results for these materials. A conjugate gradient technique was used to minimize the Hohenberg-Kohn total energy functional,[11] and the exchange and correlation effects were treated within the local density approximation (LDA) in the Perdew-Zunger parameterization of the Ceperley-Alder data.[12] The positions of the ions were determined by minimizing the atomic forces using a variable-metric scheme.[13] The surfaces were considered to be fully relaxed when the forces on the ions were less than 0.01 eV/Å.

B. Surface and slab geometries

$BaTiO_3$ and $PbTiO_3$ both belong to the group of II–IV perovskite compounds, i.e., ABO_3 perovskites in which atoms A and B are divalent and tetravalent, respectively. In this case, the AO and BO_2 layers are charge-neutral, so that both AO– and BO_2–terminated surfaces are nonpolar.

The surfaces have been represented by periodically repeated slabs consisting of 7–9 alternately stacked layers of AO and TiO_2. Both types of surface terminations have been considered, and the slabs were separated by a vacuum region of two lattice constants. A (4,4,2) Monkhorst/Pack k-point mesh[14] was used for all Brillouin-zone integrations. As has been stated in Ref. 4, the results for structural properties of perovskite surfaces are very well converged for this choice of the supercell geometry and k-point mesh.

$BaTiO_3$ and $PbTiO_3$ display different sequences of structural phase transitions as the temperature is lowered. $PbTiO_3$ undergoes a single transition from a cubic paraelectric to a tetragonal ferroelectric phase at 763 K, which is the ground state structure at T=0. $BaTiO_3$ displays a series of three transitions from cubic paraelectric to tetragonal, orthorhombic, and rhombohedral ferroelectric phases at 403 K, 278 K, and 183 K, respectively.

Because we are primarily interested in the situation where a material shows a polarization perpendicular to the surface, we focus here on the tetragonal FE phases of $BaTiO_3$ and $PbTiO_3$, and we consider only the case of the tetragonal c axis pointing perpendicular to the surface (in the following referred to as the z direction). To prevent $BaTiO_3$ from adopting the true rhombohedral T=0 structure, mirror symmetries M_x and M_y have been imposed during the relaxation of the atoms, thus mimicking the experimental room-temperature structure. In other words, only displacements of the atoms in the z direction (perpendicular to the surface) were allowed. This also prevents the polarization from rotating to become parallel to the surface. Additionally, the slab lattice constant in the x and y directions was set equal to the theoretical equilibrium lattice constant a computed for the bulk tetragonal phase (a=3.94 Å and c=3.99 Å for $BaTiO_3$, and a=3.86 Å and c=4.04 Å for $PbTiO_3$).

C. Electrical boundary conditions

For slabs with a net polarization perpendicular to the surface, two questions have to be addressed: (i) What are the appropriate boundary conditions for the electrostatic potential in the FE state? (ii) How will the electrostatic potential be modified by the periodic repetition of the slabs?

1. Boundary conditions in the FE state

Let us first consider an *isolated* slab with a polarization perpendicular to the surfaces. We choose the surface normal $\hat{\mathbf{n}}$ to be parallel to the z–axis, and we assume the charge density $\rho(\mathbf{r})$ of the slab to be periodic in the x– and y–direction. The polarized slab exhibits an electric dipole moment

$$m = \int_{-\infty}^{\infty} \bar{\rho}(z)\, z \, \mathrm{d}z \tag{1}$$

parallel to the surface normal $\hat{\mathbf{n}}$, where $\bar{\rho}(z)$ is the planar averaged charge density

$$\bar{\rho}(z) = \frac{1}{A} \iint_A \rho(\mathbf{r})\, \mathrm{d}x\, \mathrm{d}y \quad , \tag{2}$$

and A is the area of the surface unit cell. The electrostatic potential $v(\mathbf{r})$ seen by the electrons can be calculated by solving the Poisson equation

$$\nabla^2 v(\mathbf{r}) = 4\pi e\, \rho(\mathbf{r}) \quad . \tag{3}$$

In addition to the microscopic quantities $\rho(\mathbf{r})$ and $v(\mathbf{r})$, we assume the slabs to be thick enough that also macroscopic quantities like the macroscopic electric field $\mathbf{E}$, the dielectric displacement field $\mathbf{D}$, and the polarization $\mathbf{P}$ are well defined inside the slab. In practice, these fields may be calculated, for example, from unit cell averages of the electrostatic potential and the charge density.[6] However, we will see that for slabs with only 7–9 atomic layers, the applicability of this approach has its limitations.

In the case of an applied external electric field $\mathbf{E}_{\mathrm{ext}}$ perpendicular to the surfaces, the dielectric displacement field $\mathbf{D}$ inside the slab is oriented parallel to the z–axis and is equal to $\mathbf{E}_{\mathrm{ext}}$. The boundary condition of a vanishing external electric field is therefore equivalent to a vanishing dielectric displacement field $\mathbf{D}$ inside the slab. Figure 1(a) shows a schematic picture of the planar-averaged potential $\bar{v}(z)$ for this situation. The potential is constant outside the slab, but due to the slab dipole moment m, the potential jumps by $4\pi e m$ when going from one side of the slab to the other. At the same time, the polarization $\mathbf{P}$ leads to surface charges $\sigma = \mathbf{P}\cdot\hat{\mathbf{n}}$ which give rise to a huge depolarization field $\mathbf{E} = \mathbf{D} - 4\pi\mathbf{P} = -4\pi\mathbf{P}$ inside the slab (notice that $\mathbf{E}$ does not depend on the thickness of the slab). The contribution of the depolarization field to the total energy is large enough to completely destabilize the bulk FE state.[15,16] Therefore, relaxing a polarized slab under the boundary condition of a vanishing external electric field will inevitably result in a paraelectric cubic structure.

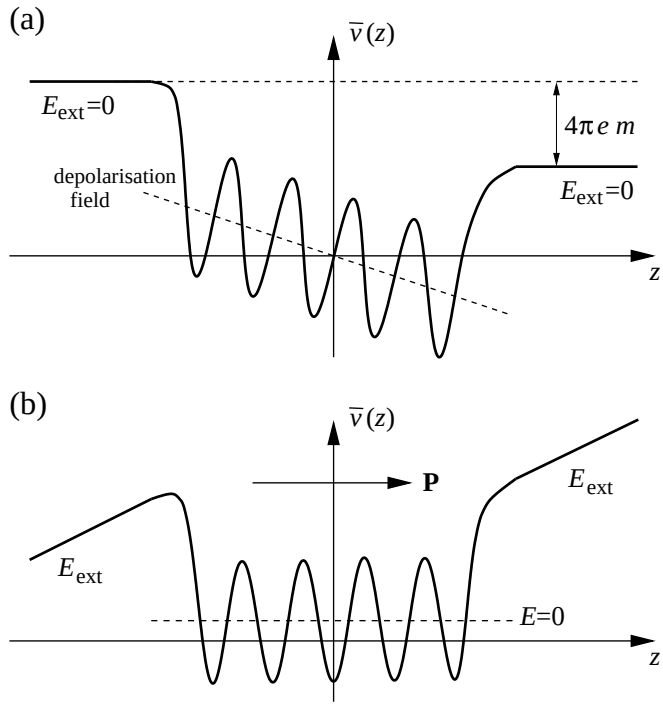

FIG. 1. Schematic illustration of the planar-averaged potential $\bar{v}(z)$ for an isolated slab with a dipole moment m perpendicular to the surface. (a) Vanishing external electric field (equivalent to D=0). (b) Vanishing internal electric field (E=0).

A comparison with the situation in an infinitely extended crystal shows which boundary conditions have to be used instead. In DFT calculations for bulk systems, periodic boundary conditions for the electrostatic potential are usually applied. In this case, the internal electric field $\mathbf{E}$ vanishes, even in the presence of a spontaneous polarization $\mathbf{P}_{\mathrm{s}}^{\mathrm{bulk}}$, whereas the dielectric displacement field $\mathbf{D}$ will be nonzero. In analogy, a slab is in a FE state with spontaneous polarization $\mathbf{P}_{\mathrm{s}}$ if a situation exists where the internal electric field $\mathbf{E}$ is zero, but the dielectric displacement field $\mathbf{D}$ is nonzero. However, an external electric field $\mathbf{E}_{\mathrm{ext}} = \mathbf{D} = 4\pi\mathbf{P}_{\mathrm{s}}$ will then appear outside the slab, as shown in Fig. 1(b).

In our calculations we are only able to control the external electric field $\mathbf{E}_{\mathrm{ext}}$ but not the internal field $\mathbf{E}$. So to study whether a slab shows a FE instability, we have to apply external electric fields of different strength and search for the situation where $\mathbf{E} = \mathbf{E}_{\mathrm{ext}} - 4\pi\mathbf{P}$ is zero. A rough estimate of how large $\mathbf{E}_{\mathrm{ext}}$ will be in this situation can be made if we assume that the polarization of the slabs is equal to the bulk spontaneous polarization

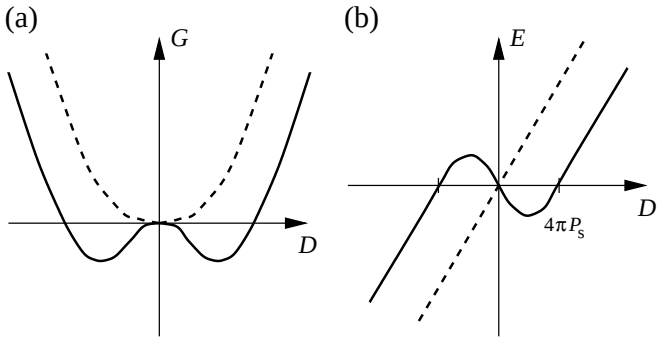

FIG. 2. Sketch of the Gibbs free energy G and the internal electric field E as a function of the dielectric displacement D (or the external electric field $E_{\rm ext}$, respectively) for a paraelectric (dotted line) or ferroelectric (solid line) slab.

$\mathbf{P}_{\rm s}^{\rm bulk}$. By using the Berry phase approach,[17] we have calculated the bulk spontaneous polarization of $BaTiO_3$ and $PbTiO_3$ to be 4.6×10^{-3} e/bohr^2 and 14.2×10^{-3} e/bohr^2, respectively. This translates to external electric fields of 0.058 a.u. and 0.18 a.u. (atomic units are used throughout the paper[18]).

To be able to distinguish between a paraelectric or ferroelectric behavior of a slab, we employ a simple phenomenological picture. We introduce the elastic Gibbs energy[15] $G(\mathbf{D})$ and we concentrate only on the dependence on the dielectric displacement field $\mathbf{D}$ (neglecting temperature and strain effects this is just the internal energy U). For a paraelectric, $G(\mathbf{D})$ is roughly quadratic in $\mathbf{D}$, whereas for a FE material $G(\mathbf{D})$ will show the well known double-well structure (see Fig. 2(a)). Differentiating the Gibbs function gives immediately the internal electric field

$$\mathbf{E} = \frac{\partial G}{\partial \mathbf{D}} \quad . \tag{4}$$

Thus, calculating $\mathbf{E}(\mathbf{D})$ directly reveals whether a slab is FE or not (see Fig. 2(b)). For a paraelectric slab, $\mathbf{E}$ is proportional to $\mathbf{D}$, with the proportionality factor given by the reciprocal dielectric constant, for a ferroelectric, the internal electric field is first negative as the polarization builds up, and then vanishes when the spontaneous polarization $\mathbf{P}_{\rm s}$ is reached. We will make use of this kind of analysis later in Secs. III B and III C 3.

2. *Periodically repeated supercells*

In supercell calculations, periodic boundary conditions are usually imposed on the electrostatic potential. For slabs with a non-vanishing dipole moment perpendicular to the surface, this leads to electrostatic potentials that typically look like the sketch shown in Fig. 3(a). The electrostatic potential corresponds neither to the situation of Fig. 1(a) nor Fig. 1(b). Instead, the imposition of

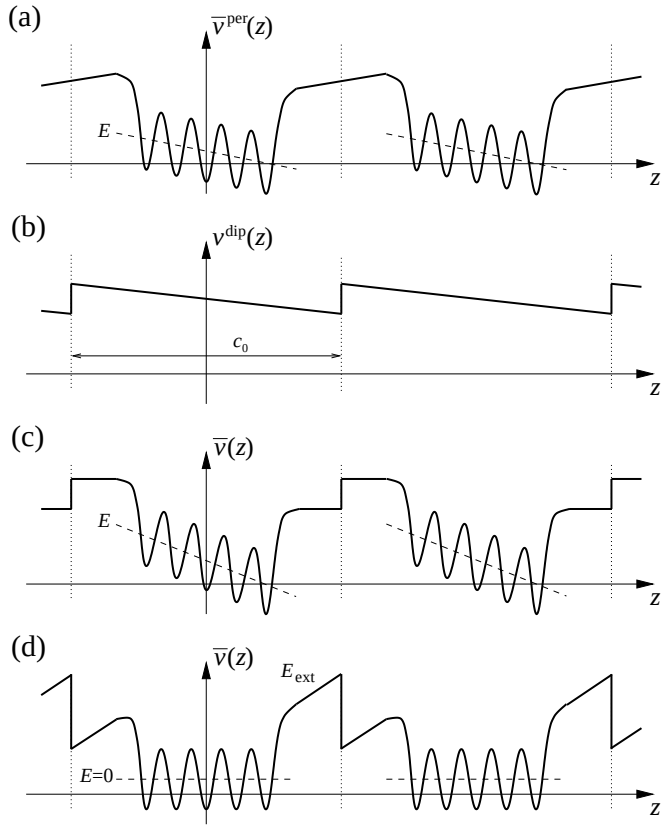

FIG. 3. Schematic picture of the planar averaged potential $\bar{v}(z)$ for periodically repeated slabs. (a) with periodic boundary conditions, (b) potential of the dipole layer, (c) dipole corrected slabs with vanishing external electric field, (d) dipole corrected slabs with vanishing internal electric field.

periodic boundary conditions on the supercell geometry leads to some other particular combination of internal and external electric fields, such that there is no discontinuity in the potential at the supercell boundary. The same occurs even for paraelectric slabs when terminated by nonequivalent surfaces with different work functions.

The artificial electric fields become smaller when the thickness of the slab or the vacuum region is increased, but it is computationally very expensive to converge results by using larger and larger supercells. Fortunately, the error associated with the artificial electric field can easily be eliminated by introducing an external dipole layer in the vacuum region of the supercell.[19,20] The electrostatic potential of this dipole layer is shown in Fig. 3(b). In order to reach a situation corresponding to Fig. 1(a), the unwanted artificial external electric field can be compensated by *adding* a certain amount of the potential of Fig. 3(b) to that of Fig. 3(a), as is shown in Fig. 3(c) (dipole correction[19]). The dipole-corrected electrostatic potential is now discontinuous, but the discontinuity lies in the vacuum region of the supercell where the wave functions are essentially zero. Alternatively, the external dipole layer may be used to apply a true exter-

nal electric field $\mathbf{E}_{\rm ext}$ to the surfaces.[20] In particular, the situation of Fig. 1(b) can be reached by *subtracting* a certain amount of the dipole potential of Fig. 3(b) from that of Fig. 3(a), as shown in Fig. 3(d).

The external dipole field can easily be implemented in any plane-wave based electronic structure code. Following the notation of Bengtsson,[19] we denote the external dipole potential of Fig. 3(b) as $v^{\rm dip}(z)$, and the electrostatic potential for the electrons calculated under periodic boundary conditions (corresponding to Fig. 3(a)) as $v^{\rm per}(\mathbf{r})$. The new potential is then

$$v(\mathbf{r}) = v^{\rm per}(\mathbf{r}) + v^{\rm dip}(z) \quad . \tag{5}$$

For a slab with dipole moment m and an external electric field $E_{\rm ext}$, the dipole potential is given by

$$v^{\rm dip}(z) = -e\left(\frac{4\pi m}{c_0} - E_{\rm ext}\right) z \quad , \quad -\frac{c_0}{2} < z < \frac{c_0}{2} \quad , \tag{6}$$

where c_0 is the height of the supercell. In a self-consistent calculation, the charge density, and thereby m, change with each step of the iteration. Therefore, m and the dipole potential $v^{\rm dip}(z)$ have to be recalculated on each iteration until self-consistency is achieved (analogous to the updating of the Hartree and the exchange-correlation potentials).

The additional external potential $v^{\rm dip}(z)$ also leads to changes in the total energies $E_{\rm tot}$ and the Hellmann-Feynman forces $\mathbf{F}_I$:

$$E_{\rm tot} = E_{\rm tot}^{\rm per} + \left(\frac{2\pi m}{c_0} - E_{\rm ext}\right) A\, m \quad , \tag{7}$$

$$\mathbf{F}_I = \mathbf{F}_I^{\rm per} - e Z_I \left(\frac{4\pi m}{c_0} - E_{\rm ext}\right) \hat{\mathbf{e}}_z \quad , \tag{8}$$

where $E_{\rm tot}^{\rm per}$ and $\mathbf{F}_I^{\rm per}$ are the total energy and Hellmann-Feynman force calculated with the periodic potential $v^{\rm per}(\mathbf{r})$, and Z_I is the ionic charge of ion I.

III. RESULTS AND DISCUSSION

A. Zero external electric field

As a first step, we calculated the fully relaxed structure of the various slabs in zero external electric field. For the asymmetrically terminated 8-layer slabs, the dipole correction was used to enforce the vanishing of the external field. In this case, as has been pointed out in Sec. II C 1, all slabs adopt the paraelectric cubic phase. The symmetrically terminated slabs show no dipole moment (the central layer of the slabs is a mirror plane), and the small dipole moment of the asymmetrically terminated slabs is solely caused by the difference between the work functions of the two surfaces.

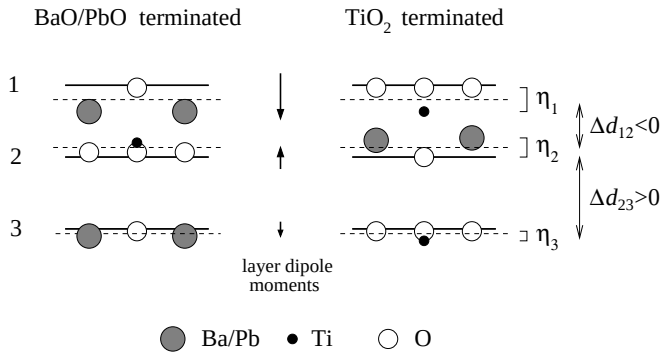

FIG. 4. Schematic illustration of the structure of the first three surface layers.

Detailed results on the structure of the $BaTiO_3$ and $PbTiO_3$ surfaces in the cubic phase in the absence of an external electric field have already been published in Refs. 3 and 4. Therefore, we give here only a brief summary in order to establish notation and to provide a baseline for comparison.

Figure 4 shows a schematic illustration of the structure of the first three surface layers, where the relaxations of the atoms have been highly exaggerated. For both $BaTiO_3$ and $PbTiO_3$, and for both the BaO/PbO and TiO_2 surface terminations, the same characteristic features appear regarding the buckling of the surface layers and the changes of the interlayer distances. Only the amplitudes of these relaxations differ from surface to surface. For a quantitative analysis of the surface relaxations, we let $\delta_z(\mathrm{O}_i)$ and $\delta_z(\mathrm{M}_i)$ be the displacements of the oxygen and metal atoms, respectively, relative to the ideal unrelaxed structure in layer i. The change of the interlayer distance Δd_{ij} is then given by the difference of the averaged displacements $(\delta_z(\mathrm{M})+\delta_z(\mathrm{O}))/2$ of the atoms in layers i and j. For all surfaces, Δd_{12} is negative (corresponding to a reduction of the interlayer distance between the first and the second surface layer compared to the bulk value), whereas Δd_{23} is positive. To describe the buckling of the surface layers, we define a rumpling parameter η_i as the amplitude of the relative displacements between the metal and the oxygen ions: $(\delta_z(\mathrm{M}_i)-\delta_z(\mathrm{O}_i))$. η_i is negative if the metal ions are below the oxygen atoms, which is true for the first surface layer of all surfaces. For the next surface layers, η_i oscillates in sign from layer to layer, and the amplitude decreases very rapidly.

B. External electric field without field-induced atomic relaxations

In the next step, we exposed the slabs to external electric fields $\mathbf{E}_{\rm ext}$ of increasing strength, but we kept all atoms frozen in the positions which have been calculated in zero external field. Only the distribution of the elec-

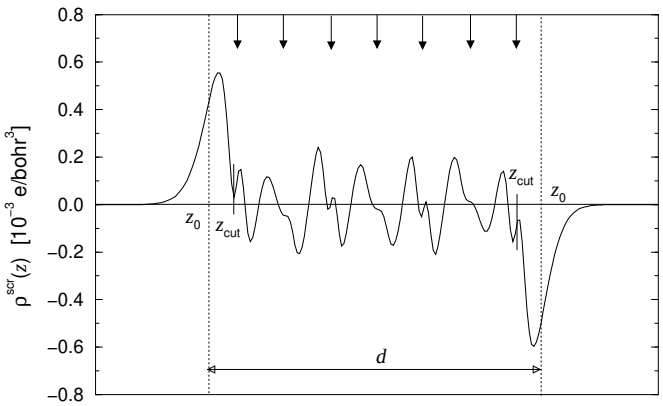

FIG. 5. Planar-averaged screening charge distribution of a BaO–terminated slab of $BaTiO_3$, calculated from a 7-layer slab for an electric field of $E_{\rm ext}$=+0.02 a.u. The arrows indicate the positions of the atomic planes. "Top" of slab is at right.

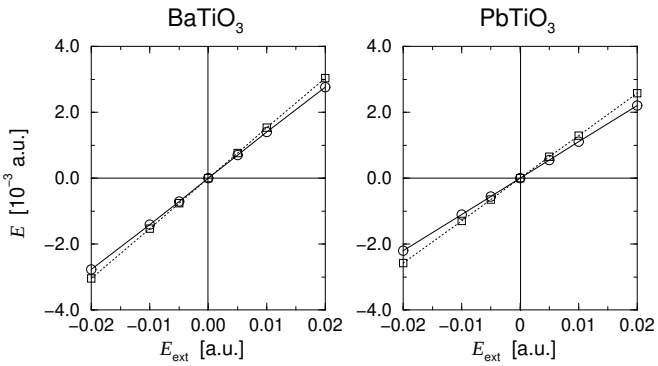

FIG. 6. Internal electric field E in the 7-layer slab with frozen atomic positions as a function of the applied external electric field $E_{\rm ext}$. Solid lines: AO–terminated slabs. Dotted lines: TiO_2–terminated slabs. Atomic units are used.[18]

	$BaTiO_3$		$PbTiO_3$	
	BaO–term.	TiO_2–term.	PbO–term.	TiO_2–term.
7	7.1	6.5	9.0	7.7
8			8.1	
9	7.0	6.6		
bulk	6.75		8.24	

TABLE I. Calculated optical dielectric constants ϵ_∞ for the various slabs. The theoretical bulk values are taken from Ref. 21.

trons was recalculated self-consistently. This mimics the exposure of the slabs to a AC electric field with a frequency high enough that the ions are no longer able to follow. In this situation, we expect the slabs to show a purely paraelectric response. That is, a linear relation between the internal electric field $\mathbf{E}$ and the dielectric displacement field $\mathbf{D}$ should be found, $\mathbf{D}=\epsilon_\infty\mathbf{E}$, where ϵ_∞ is the optical dielectric constant.

To verify this, we calculated the internal electric field $\mathbf{E}$ as a function of the applied external electric field $\mathbf{E}_{\rm ext}$ (or, equivalently, the dielectric displacement field $\mathbf{D}$). A natural way to compute $\mathbf{E}$ would be to determine the gradient of the macroscopically averaged electrostatic potential $v(\mathbf{r})$. Unfortunaly, it turned out that 7–9 layers are not enough to give accurate macroscopic averages (the uncertainties in the gradients were much too large). Instead, we calculated the internal electric field by using the relation $\mathbf{E}=\mathbf{D}-4\pi\mathbf{P}$. The polarization $\mathbf{P}$ can either be deduced from the surface charge σ or from the dipole moment m and the thickness d of the slabs:

$$P = \sigma \quad , \qquad P = m/d \quad . \tag{9}$$

The dipole moment m is directly given by the charge distribution of the slabs via Eq. (1). For the thickness d we have taken the distance between the centers of gravity z_0 of the screening charge distribution of the top and bottom surface of our slabs. (For a metal, z_0 is the position of the surface image plane from which the classical image potential is measured.) The screening charge distribution is given by the difference of the charge densities calculated with and without an external electric field. A typical planar-averaged screening charge distribution $\bar{\rho}^{\rm scr}(z)$ is shown in Fig. 5. As expected, a positively-oriented electric field pushes the electrons into the slab at the top surface and pulls them out at the bottom (where it can be interpreted as a negatively-oriented field). From Fig. 5, we see that the screening charge piles up directly at the surface and is mainly confined above the surface atoms. These surface charges are responsible for the screening of the external electric field. Inside the slab, fairly large oscillations are found which are associated with the remaining internal electric field.

The surface charge σ and the center of gravity of the screening charge distribution z_0 for the top surface of the slab are given by

$$\sigma = \int_{z_{\rm cut}}^{c_0/2} \bar{\rho}^{\rm scr}(z)\, {\rm d}z \quad , \qquad z_0 = \frac{1}{\sigma}\int_{z_{\rm cut}}^{c_0/2} \bar{\rho}^{\rm scr}(z)\, z\, {\rm d}z \quad . \tag{10}$$

For $z_{\rm cut}$ we have taken the position where the extrapolation of the first charge peak goes to zero (see Fig. 5), but the results are not very sensitive to the choice of $z_{\rm cut}$. Analogous relations apply for the bottom surface. To check the consistency of this approach, we have calculated the polarization $\mathbf{P}$ of the slabs in both of the ways indicated in Eq. (9), i.e., using either the surface charges σ or the dipole moment m with the thickness d. In all cases, the computed values for the polarization differ by less than 1%.

With the polarization $\mathbf{P}$ we can finally determine the internal electric field $\mathbf{E}$. Figure 6 shows the internal electric field for the 7-layer slabs as a function of the applied external field. Compared with our phenomenological picture in Fig. 2, a clear paraelectric behavior can be seen for all slabs. Table I gives the optical dielectric constants

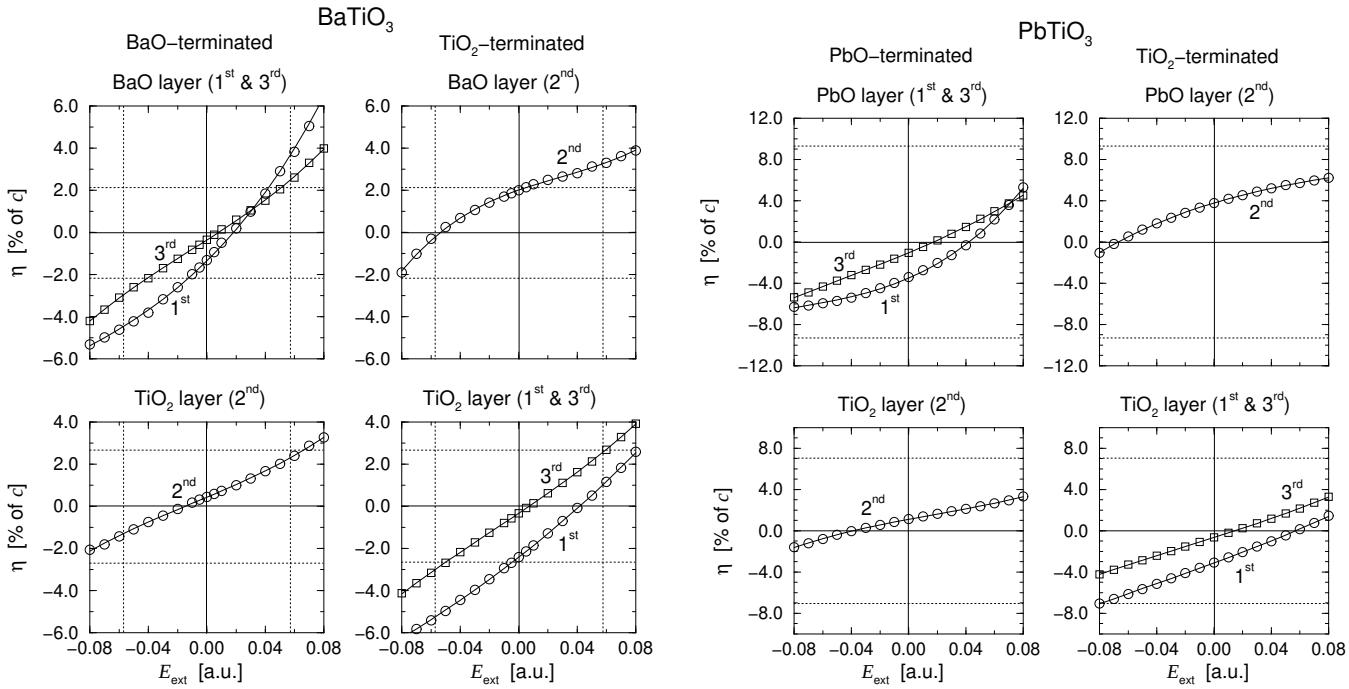

FIG. 7. Field dependence of the rumpling parameter η_i calculated from the 7-layer slab. Dotted horizontal lines: amplitude of displacement of metal and oxygen ions in the bulk ferroelectric state. Dotted vertical lines: External electric field corresponding to the bulk spontaneous polarization.

deduced from the $E(D)$ plots for the different slabs, together with the LDA bulk values of Ref. 21. Already for 7 atomic layers, the dielectric constants agree very well with the bulk values. The finite-size effect is less than 10%. Its sign depends on the relative numbers of AO and TiO_2 layers: ϵ_∞ is increased when the number of AO–layers exceeds the number of TiO_2–layers, and is reduced when the slabs contain more TiO_2 layers.

C. External electric field with atomic relaxations

Finally, all slabs were fully relaxed in the presence of external static electric fields. Fields of strength varying between -0.08 a.u. and $+0.08$ a.u. have been applied. Starting from zero field, the amplitude of the field was changed in steps of 0.01 a.u., and the atomic positions at the previous field were used as initial configurations for the new atomic relaxations. The upper limit of 0.08 a.u. for the amplitude of the external electric field is determined in our calculations by the thickness of the vacuum region for the following reason. As can be seen in Fig. 3(d), there is a kind of "quantum well" located in the vacuum region just to the right of the dipole layer. If the electrostatic potential of this quantum well drops below the Fermi level, it can become populated by the transfer of electrons from the slab region. The threshold for the occurrence of this unwanted behavior depends on both the width of the vacuum region and the strength of the electric field.

1. Field-induced atomic relaxations

In a positively oriented external electric field, the negatively charged oxygen ions will be pushed into the bulk and the positive ions will be pulled towards the surface. This will immediately change the rumpling parameter η_i of the surface layers, as can be seen in Fig. 7. For small applied fields, η_i increases linearly with the strength of $E_{\rm ext}$, as is expected if a harmonic coupling between the atoms is assumed. However, for larger fields, nonlinear effects become important, especially for the first and second AO layers.

To facilitate comparison of these surface rumplings with the corresponding bulk rumplings of the "up" and "down" FE states, the latter are drawn as horizontal dotted lines in Fig. 7. That is, these lines show the values that the rumpling parameters would have if the corresponding slab had been a piece of truncated FE bulk material without any further relaxation of the atoms. Additionally, for $BaTiO_3$ we have used dotted vertical lines to indicate the magnitude of the external electric field $\mathbf{E}_{\rm ext}=4\pi\mathbf{P}_{\rm s}^{\rm bulk}$ that would be consistent with a bulk spontaneous polarization $\mathbf{P}_{\rm s}^{\rm bulk}$ in the interior of the slab.

It can be seen from Fig. 7 that for this external electric field, the rumpling parameters η_i of the surface layers have reached the same order of magnitude as the bulk FE distortions. For most layers η_i is slightly larger, but for some layers it is a little bit smaller. Overall, the rumpling parameter η_i tends to be larger for the negative electric field than for the positive field, suggesting

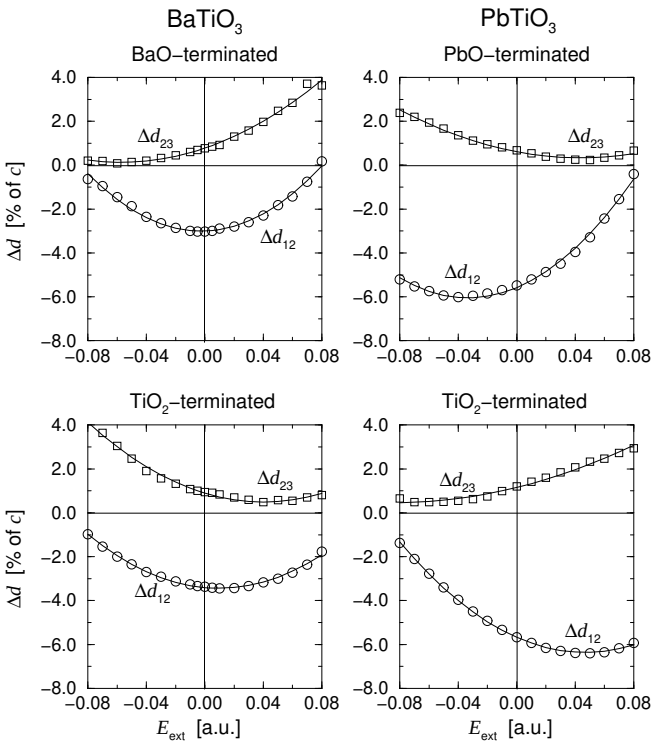

FIG. 8. Field-dependence of the change in interlayer distances Δd_{ij} calculated for the 7-layer slabs.

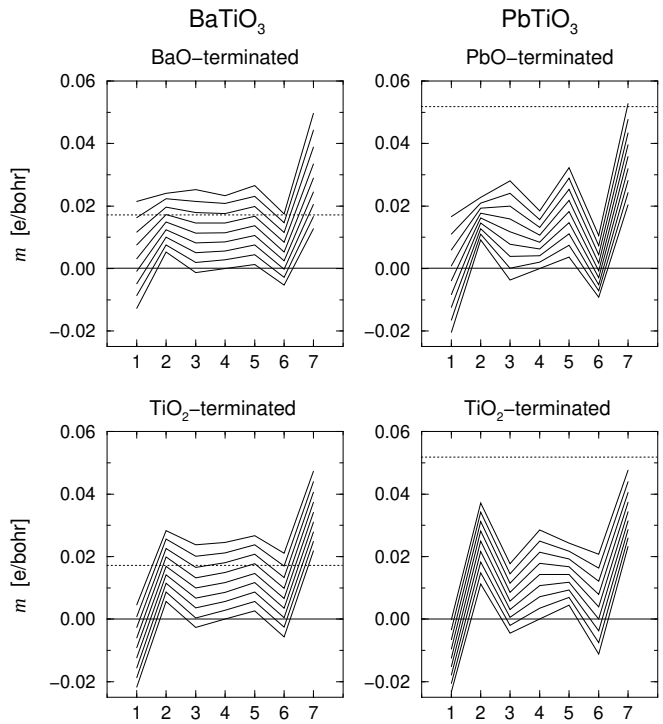

FIG. 9. Dipole moment per atomic layer calculated for the 7-layer slabs for electric fields from 0 to 0.08 a.u. in steps of 0.01 a.u. The orientation of the electric field corresponds to a positive field for the top surface and a negative field for the bottom surface. The dotted line represents the dipole moment for an atomic layer in the bulk ferroelectric state, calculated from the bulk spontaneous polarization via $c/2{\cdot}P_{\rm s}^{\rm bulk}$.

that the surface polarization is larger for the negatively-oriented field. However, it is difficult to deduce from Fig. 7 whether the polarization is enhanced or reduced at the surface compared with the bulk. We will return to this question in the next subsection.

The bulk spontaneous polarization $\mathbf{P}_{\rm s}^{\rm bulk}$ is roughly three times larger for $PbTiO_3$ than for $BaTiO_3$ (see Section II C 1). The external electric field for the case that a slab adopts the $PbTiO_3$ bulk spontaneous polarization is therefore on the order of 0.18 a.u. This is well beyond the upper limit of the electric field that can be applied in our calculations. Consequently, the polarization of the $PbTiO_3$ slabs is well below $\mathbf{P}_{\rm s}^{\rm bulk}$ for all applied external electric fields, and therefore it is no surprise that the surface rumpling η_i in Fig. 7 is much smaller than the corresponding bulk FE rumpling over the entire range of accessible external electric fields.

Associated with the changes in the layer rumplings, we also observe changes in the interlayer distances as shown in Fig. 8. (Note that the atomic layers are charge-neutral, so that there is no net force on the layers in an external electric field.) We find some noteworthy qualitative differences in the behaviors of the two materials (e.g., in the slopes of the Δd_{23} *vs.* $E_{\rm ext}$ curves). Ultimately these differences can presumably be traced to the rather different chemistry of Ba–O and Pb–O bonds, but a detailed explanation of the observed trends is not obvious.

2. *Field-induced layer dipoles*

To address the question how the polarization is changed at the surface, we have subdivided the total dipole moment m of the slabs from Eq. (1) into dipole moments m_i per atomic layer. This was done by identifying the "nodes" z_i at which $\int_{-c_0/2}^{z_i} \bar{\rho}(z)\,{\rm d}z$ vanishes. Regions between successive nodes are thus charge neutral and contain exactly one AO or TiO_2 atomic plane. The dipole moment m_i was then calculated via Eq. (1) while restricting the range of integration to the area between the two nodes which embrace the atomic layer of interest.

Fig. 9 shows the dipole moments per atomic layer for the 7-layer slab in different external electric fields. For zero external electric field, the dipole moments oscillate in sign from layer to layer. The dipole moment is largest for the first atomic layer at the surface and goes to zero very rapidly (see also Fig. 4). Finally, the net dipole moment of the surface, given by the sum of the m_i of all surface layers, points inwards towards the bulk for all surfaces.

An external electric field causes the dipole moments of all layers in the slab to increase more or less equally. The dipole moments continue to oscillate from layer to layer

	dipole moment		polarization			
	AO–term.	TiO_2–term.	AO–term.		TiO_2–term.	
$SrTiO_3$	−8.7	−14.2	1.19	(–)	1.95	(–)
$BaTiO_3$	−7.4	−14.7	0.98	(21%)	1.95	(42%)
$PbTiO_3$	−11.3	−11.8	1.48	(10%)	1.55	(11%)

TABLE II. Dipole moment (in 10^{-3}e/bohr) and polarization (in 10^{-3}e/bohr^2) of the surface unit cell as calculated from the 7-layer slabs.[18] The surface polarization as a fraction of the theoretical bulk spontaneous polarization is given in parentheses. Values for $SrTiO_3$ are given for comparison.

when $E_{\rm ext}$ is increased, but they approach a constant bulk value already after two layers in $BaTiO_3$ and after three layers in $PbTiO_3$. (This becomes more apparent from the 8- and 9-layer slab calculations, not shown here.) The dipole moments in the surface layers are modified relative to the bulk layers by the inwards oriented surface dipoles. This leads to a suppression of the polarization at the surface in a positively-oriented external electric field, and an enhancement for a negative field. However, the modification of the polarization is more or less confined to the first unit cell (i.e., first pair of layers) at the surface.

In most cases a rough estimate of how much the polarization is suppressed or enhanced at the surface is given by the surface dipole moments in zero external electric field. Table II lists the dipole moment of the uppermost unit cell (i.e., the sum of the dipole moments m_i of the first two atomic layers) in zero external electric field for slabs of 7 layers. (The results from 8- and 9-layer slabs differ by less than 3%.) Additionally, these dipole moments have been converted to a polarization by dividing them by the lattice constant c.

The values of the dipole moments of the uppermost unit cells are of the same order of magnitude for all surfaces. In the case of $BaTiO_3$, they correspond to about 20–40% of the bulk spontaneous polarization $\mathbf{P}_{\rm s}^{\rm bulk}$. Therefore, for $BaTiO_3$ a relatively large change in the polarization at the surface has to be expected for a spontaneously polarized slab. On the other hand, for $PbTiO_3$ the surface dipoles make up only about 10% of the bulk spontaneous polarization. The modification of the polarization at the surface in a spontaneously polarized state will therefore be only modest. The polarization will be suppressed for an upwards polarization and enhanced for a downwards polarized state.

3. Ferroelectric instability of the slabs

The results presented so far on the structure of the surfaces do not provide an answer to the question whether the slabs exhibit a true FE instability or simply show a paraelectric polarization. Instead, we have to determine the electric field inside the slabs as a function of the applied external field and compare the result with our simple phenomenological picture from Fig. 2(b).

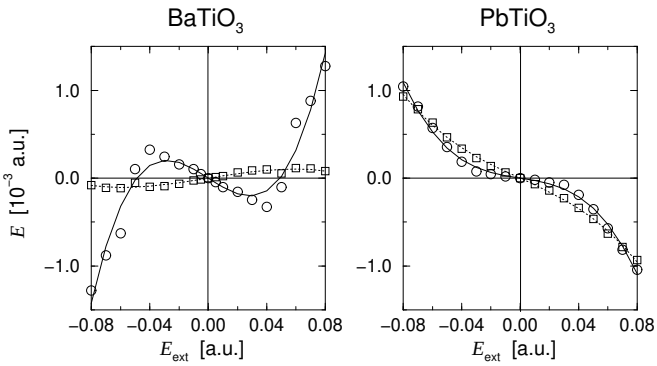

FIG. 10. Internal electric field E in the fully relaxed 7-layer slab as a function of the applied external electric field $E_{\rm ext}$. Solid lines, AO–terminated slabs; dotted lines, TiO_2–terminated slabs.

For the calculation of the internal electric field we followed the same procedure as described in Section III B. However, instead of using the true screening charge distribution (which includes contributions from the moving ions) to determine z_0 and d, we took the difference between the charge density of the fully relaxed slab in the external electric field and the charge density of a calculation where the atomic positions have been kept fixed and the electric field turned off. Unfortunately it turned out that it is not possible to determine the internal electric field to very high precision. The use of the relation $\mathbf{E}=\mathbf{D}-4\pi\mathbf{P}$ involves the difference of two relatively large numbers, so that the result for the internal electric field depends very sensitive on details of the calculation. In particular, the determination of the thickness d of the slabs is very critical. Also when approaching the breakdown field above which electrons accumulate in the quantum well next to the dipole layer, the wavefunctions start to penetrate the barrier between the slab and the quantum well. This leads to a small overestimation of the dipole moment and the polarization of the slab at high applied fields. But because of the subtle difference between the external electric field and the polarization, the error in the internal electric field becomes noticable, and deviations from the behavior described in Fig. 2(b) may appear at large external fields. Therefore, the curves of the internal electric field as a function of the applied external electric field shown in Fig. 10 represent only basic tendencies but are not to be taken as quantitatively accurate results.

The results in Fig. 10 are clearest for the BaO–terminated slab of $BaTiO_3$, where the full curve expected for ferroelectric behavior, as in Fig. 2(b), can be observed. We find that the internal electric field vanishes for an external electric field of approximately 0.05 a.u. (the result for the 9-layer slab is the same). This translates to a spontaneous polarization of the slab of $P_{\rm s}=4\times10^{-3}$ e/bohr^2, which corresponds roughly with the bulk spontaneous polarization $\mathbf{P}_{\rm s}^{\rm bulk}$ of $BaTiO_3$. How-

ever, due to the limitations in the accuracy of our calculations, we are not able to say for certain whether the spontaneous polarization of the slab is enhanced or reduced compared to the bulk value.

For the other three cases in Fig. 10 it is more difficult to deduce, whether the slabs show a FE instability or not. For $PbTiO_3$ we have the problem that the upper limit for the external electric field is reached long before the slabs come close to a polarization equal to the bulk spontaneous polarization (as has been pointed out above). In Fig. 10, the external electric field where the internal field is zero can therefore not be reached for the $PbTiO_3$ slabs.

On the other hand, according to Fig. 2(b), a negative slope of the internal electric field at zero applied field is already a very good indicator for a FE instability. As can be seen from Fig. 10, this condition is fulfilled for both the PbO–terminated and the TiO_2–terminated slab of $PbTiO_3$, but not for the TiO_2–terminated slab of $BaTiO_3$. To estimate how sensitive this result depends on details of our calculations we compare the numerical values of the initial slopes of the $E(D)$ curves with an error bar which we derive from the uncertainties in the determination of the slab thickness d. The fit curves in Fig. 10 yield initial slops of -9.1×10^{-3} and $+2.6\times10^{-3}$ for the BaO– and TiO_2–terminated $BaTiO_3$ slabs and -2.5×10^{-3} and -7.6×10^{-3} for the PbO– and TiO_2–terminated $PbTiO_3$ slabs, respectively. By varying $z_{\rm cut}$ in Eq. (10) we can estimate an error bar of about $\pm4\times10^{-3}$. For the BaO–terminated $BaTiO_3$ slab and the TiO_2–terminated $PbTiO_3$ slab the initial slopes are well outside the error bar, indicating a ferroelectric instability of the slabs, whereas for the TiO_2–terminated $BaTiO_3$ slab and the PbO–terminated $PbTiO_3$ slab our analysis of the internal electric field is not accurate enough to make a clear statement. It would be possible to clarify the situation in the last two cases by going to thicker slabs with more atomic layers, since then the thickness d would be relatively less uncertain, but this was deemed too computationally demanding to be undertaken in the current project. At least we can say that both slabs are very close to a ferroelectric instability.

IV. SUMMARY

By using first-principles density-functional calculations, we have studied (001)-oriented slabs of $BaTiO_3$ and $PbTiO_3$ in external electric fields. Artificial electric fields introduced by the periodic boundary conditions of the supercell approach have been eliminated with the help of an external dipole layer in the vacuum region. In this way it is possible to handle periodically repeated polarized slabs as if they were genuinely isolated, without the need for large vacuum separations. This makes the dipole correction a very useful tool for all problems where slabs with nonvanishing dipole moments or inequivalent surface terminations have to be considered.

For the BaO–terminated $BaTiO_3$ slabs and the TiO_2–terminated $PbTiO_3$ slabs as thin as 7 atomic layers, we have found strong evidence for the presence of an instability to a spontaneously polarized ground state with the polarization perpendicular to the surface. This is in agreement with recent experiments[2] and a microscopic effective-Hamiltonian study.[7] However, because the latter approach does not explicitly take into account the structural relaxations at the surface, it cannot provide the detailed level of description that our theory gives. In particular, we find an enhancement of the polarization at the surface for which the polarization points inwards, whereas the polarization is reduced when the spontaneous polarization points outwards. We have also detailed the variations in these surface relaxations as the polarization of the slab is modified by an external electric field.

In order to obtain an even more realistic level of description, the next obvious step will be to calculate the influence of a real metal/perovskite interface on the atomic relaxations and the polarization at the interface. However, such a study requires the choice of a particular metallic overlayer with particular epitaxy conditions, and is thus intrinsically less universal. Nevertheless, it may be an interesting avenue for future investigation.

V. ACKNOWLEDGMENTS

We wish to thank Karin Rabe for useful discussions. This work is supported by the ONR grant N00014-97-1-0048.

[1] T. Maruyama, M. Saitoh, I. Sakai, T. Hidaka, Y. Yano, and T. Noguchi, Appl. Phys. Lett. **73**, 3524 (1998), and references therein.
[2] T. Tybell, C. Ahn, and J.-M. Triscone, Appl. Phys. Lett. **75**, 856 (1999).
[3] J. Padilla and D. Vanderbilt, Phys. Rev. B **56**, 1625 (1997).
[4] B. Meyer, J. Padilla, and D. Vanderbilt, Faraday Discuss. **114**, 395 (1999).
[5] R.E. Cohen, J. Phys. Chem. Solids **57**, 1393 (1996); R.E. Cohen, Ferroelectrics **194**, 323 (1997).
[6] L. Fu, W. Yaschenko, L, Resca, and R. Resta, Phys. Rev. B **60**, 2697 (1999).
[7] Ph. Ghosez and K.M. Rabe, Appl. Phys. Lett. **76**, 2767 (2000).
[8] J. Padilla and D. Vanderbilt, Surface Science **418**, 64 (1998).
[9] P. Hohenberg and W. Kohn, Phys. Rev. **136**, B864 (1964); W. Kohn and L.J. Sham, Phys. Rev. **140**, A1133 (1965).
[10] D. Vanderbilt, Phys. Rev. B **41**, 7892 (1990).
[11] R.D. King-Smith and D. Vanderbilt, Phys. Rev. B **49**, 5828 (1994).

[12] D.M. Ceperley and B.J. Alder, Phys. Rev. Lett. **45**, 566 (1980); J.P. Perdew and A. Zunger, Phys. Rev. B **23**, 5048 (1981).
[13] W.H. Press et al., *Numerical Recipes*, Cambridge University Press.
[14] H.J. Monkhorst and J.D. Pack, Phys. Rev. B **53**, 5188 (1976).
[15] M.E. Lines and A.M. Glass, *Principles and Applications of Ferroelectrics and Related Materials*, Clarendon Press, Oxford, 1977.
[16] W. Zhong, R.D. King-Smith, and D. Vanderbilt, Phys. Rev. Lett. **72**, 3618 (1994).
[17] R.D. King-Smith and D. Vanderbilt, Phys. Rev. B **47**, 1651 (1993).
[18] An electric field of 1 a.u. corresponds to 5.14×10^9 V/cm and a polarization of 10^{-3} e/bohr^2 equals 5.72 μC/cm^2.
[19] L. Bengtsson, Phys. Rev. B **59**, 12301 (1999).
[20] J. Neugebauer and M. Scheffler, Surface Science **287/288**, 572 (1993).
[21] U.V. Waghmare and K.M. Rabe, Phys. Rev. B **55**, 6161 (1997); Ph. Ghosez, E. Cockayne, U.V. Waghmare, and K.M. Rabe, Phys. Rev. B **60**, 836 (1999).